Mechanism and Machine Theory 198 (2024) 105654

Contents lists available at ScienceDirect

Mechanism and Machine Theory

journal homepage: www.elsevier.com/locate/mechmt

Research paper

A methodology to restrict the range of motion of joints: Application to the ankle joint complex

Mariana Rodrigues da Silva [a,b,*], Filipe Marques [a,b], Miguel Tavares da Silva [c], Paulo Flores [a,b]

[a] CMEMS-UMinho, Departamento de Engenharia Mecânica, Universidade do Minho, Campus de Azurém, Guimarães, 4804-533, Portugal
[b] LABBELS – Associate Laboratory, Braga/Guimarães, Portugal
[c] IDMEC, Instituto Superior Técnico, Universidade de Lisboa, Av. Rovisco Pais, 1, Lisboa, 1049-001, Portugal

ARTICLE INFO

Keywords:
Human foot
Ankle joint complex
Range of motion
Joint limits
Joint resistance
Multibody dynamics

ABSTRACT

One of the most critical aspects when developing biomechanical models is the formulation of the joints, which, in the case of the human body, have limited range of motion (RoM). Thus, restrictions to prevent joints from performing unacceptable movements and avoid unrealistic configurations of the adjacent bodies must be formulated. This study extends the authors' previous work to demonstrate the potential of applying a methodology to restrict the RoM of joints to the complex case of the human ankle joint complex. The methodology applies joint resistance moments to the adjacent bodies to mimic the resistive and dissipative behavior of the constituent materials and to prevent unacceptable configurations of those bodies. A detailed description of the application of the methodology to the ankle joint complex is given, including the definition of the joint's local reference frames and circumduction cones, estimation of the longitude and latitude, calculation of the maximum latitude using the elliptical approach and the transfer of forces and moments to the adjacent bodies. The methodology correctly restricts the RoM of the ankle joint complex, producing physiologically sound simulation results.

1. Introduction

Over the last decades, the use of biomechanical models to study the human movement has been increasing in many science and engineering fields [1–3], such as sports [4], clinical studies [5,6] and crashworthiness research [7,8]. A biomechanical model is a mathematical representation of the human body and can be established using different numerical approaches, namely the multibody systems methodology or the finite element method [2,9]. In the former, which is the one considered in this work, the models can be thought of as systems composed of three main ingredients, namely, a set of bodies describing large rotational and translational motions, kinematic joints constraining their relative motion, and force elements acting upon those bodies [10,11]. The validity of the results provided by the biomechanical models is strongly dependent on their computational efficiency and anatomical accuracy, such as the reliable modeling of body segments, joints, or the body-environment interaction [12,13].

One of the most critical aspects to consider when developing computational models of the human body is the formulation of the joints, which have limited range of motion (RoM). The relative amplitude of motion allowed in any joint of the human body is usually known as the RoM, and it is strongly influenced by the geometric configuration of the bony structures adjacent to the joint, as well as by

* Corresponding author.
E-mail address: m.silva@dem.uminho.pt (M. Rodrigues da Silva).

https://doi.org/10.1016/j.mechmachtheory.2024.105654
Received 16 February 2024; Received in revised form 30 March 2024; Accepted 17 April 2024
Available online 25 April 2024

Nomenclature

Latin symbols

$\mathbf{a}_i$	Unit vector perpendicular to the joint axis $\mathbf{s}_i$ belonging to body i -
a	Semi-axis of the ellipse rad
b	Semi-axis of the ellipse rad
$\mathbf{D}$	Jacobian matrix of the constraint equations -
e_0, e_1, e_2, e_3	Euler parameters -
$\mathbf{f}$	Force vector N
$\mathbf{g}$	External generalized force vector N, N·m
$\mathbf{I}$	Identity matrix -
I	Moment of inertia kg·m^2
j_h	Damping coefficient of joint h N·m·s
$\mathbf{l}$	Moment lever arm m
$\mathbf{M}$	Mass matrix kg, kg·m^2
$m_{\mathrm{p},h}$	Maximum moment magnitude to restrict the motion of joint h N·m
$\mathbf{m}$	Moment vector N·m
$\mathbf{m}_h^{\mathrm{d}}$	Joint dissipative moment vector of joint h N·m
$\mathbf{m}_h^{\mathrm{mr}}$	Joint motion-restricting moment vector of joint h N·m
$\mathbf{m}_h^{\mathrm{r}}$	Joint resistance moment vector of joint h N·m
$\mathbf{n}$	Unit vector normal to the surface of the circumduction cone -
$\dot{\mathbf{r}}_k$	Velocity vector of the center of mass of body k in global coordinates m/s
$\mathbf{s}_i$	Vector along the joint axis belonging to the reference body m
$\mathbf{s}_k^P$	Position vector of point P located on body k with respect to the center of mass in global coordinates m
t	Time variable s
$\mathbf{u}_{\mathrm{r},h}$	Unit vector defined using the moving body's local coordinate system -
$u_{\mathrm{r},h,\xi}$	Local ξ component of the unit vector $\mathbf{u}_{\mathrm{r},h}$-
$u_{\mathrm{r},h,\eta}$	Local η component of the unit vector $\mathbf{u}_{\mathrm{r},h}$ -
$u_{\mathrm{r},h,\zeta}$	Local ζ component of the unit vector $\mathbf{u}_{\mathrm{r},h}$ -
$\mathbf{u}_{\xi,h}$	Unit vector defining the ξ axis of joint h local coordinate system -
$\mathbf{u}_{\eta,h}$	Unit vector defining the η axis of joint h local coordinate system -
$\mathbf{u}_{\zeta,h}$	Unit vector defining the ζ axis of joint h local coordinate system -
$\dot{\mathbf{v}}$	Vector containing the system accelerations m/s^2, rad/s^2
xyz	Global coordinate system m

Greek symbols

α	Baumgarte stabilization coefficient -
β	Baumgarte stabilization coefficient -
$\boldsymbol{\gamma}$	Right-hand side vector of the acceleration constraint equations -
ε	Angle of the talocrural joint axis in the transverse plane rad
θ	Angle of the talocalcaneal joint axis in the sagittal plane rad
κ	Relative angular motion between the moving body and the limits of the circumduction cone rad
$\boldsymbol{\lambda}$	Lagrange multipliers vector -
ρ	Angle of the talocalcaneal joint axis in the transverse plane rad
σ_h	Latitude of joint h rad
$\sigma_{h,\max}$	Maximum allowable latitude of joint h rad
$\Delta\sigma_h$	Compliance of joint h rad
τ	Angle of the talocrural joint axis in the frontal plane rad
φ	Joint angle rad
$\boldsymbol{\Phi}$	Position constraint equations -
$\dot{\boldsymbol{\Phi}}$	Velocity constraint equations -
ψ_h	Longitude of joint h rad
$\boldsymbol{\omega}$	Angular velocity vector rad/s
$\xi\eta\zeta$	Body fixed coordinate system m
$\xi_h\eta_h\zeta_h$	Joint's local coordinate system m

Subscripts

h	Relative to a generic rotational joint h
i	Relative to body i
j	Relative to body j

p	Penalty
re	Real angle
t	Relative to time instant *t*

Superscripts

d	Relative to the dissipative moment
mr	Relative to the motion-restricting moment
r	Relative to the resistance moments

Operators

$()^{T}$	Matrix or vector transpose
$(')$	Components of a vector in a body-fixed coordinate system
$(^{'})$	Components of a vector in the joint's coordinate system
$(\sim)$	Skew-symmetric matrix of a vector
$(\|\|\ \ \|\|)$	Vector norm

the physiological properties of the surrounding soft tissues, such as muscles, tendons, and ligaments [14–18]. From the multibody systems formulation viewpoint, the kinematic joint models prevent the relative motion between interconnected bodies from occurring in the degree-of-freedom removed by the type of joint, but do not impose any restrictions on the RoM of the bodies in the degree-of-freedom allowed by the joint. Thus, additional restrictions must be formulated in order to prevent the joints from performing anatomically and physiologically unacceptable movements and to avoid unrealistic configurations of the connected bodies [18]. The RoM restriction is particularly important, for instance, in human motion simulations, in planning and optimizing the trajectories of bodies, or in the design of mobility assistive devices or exoskeletons. Thus, methodologies that realistically and accurately allow the RoM restriction are needed [19–22]. This study extends the authors' previous work [23] in order to demonstrate the potential of applying a methodology to restrict the RoM of joints to the complex case of the human ankle joint complex.

The ankle joint complex is composed of the talocrural and talocalcaneal articulations [24–26]. Plantarflexion and dorsiflexion are allowed by the talocrural articulation, which is located between the tibia and fibula, and the talus, as observed in Fig. 1. The talocalcaneal articulation allows inversion and eversion of the human foot, and it is located between the calcaneus and the talus (see Fig. 1) [27,28]. While these two articulations are the major contributors to plantarflexion, dorsiflexion, inversion and eversion, these movements are a combination of the different degrees-of-freedom of the ankle and foot in all cardinal planes. Fig. 1 shows that the talus is the bone structure inserted between the talocrural and talocalcaneal articulations, thus providing a non-coplanar rocking motion between them.

The axes of the talocrural and talocalcaneal articulations establish specific anatomical orientations between each other [29–31], as it can be observed in Fig. 2. The angles shown in Fig. 2 are projected onto the corresponding cardinal plane. Therefore, after the first rotation in one plane using the angle projected on that plane, the second rotation requires calculating the corresponding angle as the real angle between the transverse plane of the body and the joint axis. In order to determine the real angles, the following conditions must be utilized [32,33]

$$\tan\theta_{re} = \tan\theta\cos\rho \tag{1}$$

$$\tan\tau_{re} = \tan\tau\cos\varepsilon \tag{2}$$

where the subscript 're' represents the real angle. Therefore, the joint axes can be expressed as

$$\mathbf{s}_{\text{talocalcaneal}} = \{\ \cos\rho\cos\theta_{re} \quad \sin\rho\cos\theta_{re} \quad \sin\theta_{re}\ \}^{T} \tag{3}$$

$$\mathbf{s}_{\text{talocrural}} = \{\ \sin\varepsilon\cos\tau_{re} \quad \cos\varepsilon\cos\tau_{re} \quad \sin\tau_{re}\ \}^{T} \tag{4}$$

The values of ρ, θ, ε and τ can be retrieved from [18,29], and express the angles of the axes of both articulations projected onto the cardinal planes when the foot stands in the anatomical reference position, as depicted in Fig. 2.

Fig. 3 shows a schematic representation of the dorsiflexion and plantarflexion, and inversion and eversion movements of the foot provided by the talocrural and talocalcaneal joints, respectively.

The methodology utilized to restrict the RoM of joints [23] applies joint resistance moments to the bodies connected by the ankle joint complex to mimic the resistive and dissipative behaviors of the constituent materials and to prevent unacceptable configurations of those bodies. Thus, two terms contribute to the joint resistance moments, namely the dissipative and the motion-restricting terms. In this work, as an application example, a three-dimensional biomechanical model of the leg, main foot, and toes is developed using the multibody systems methodology and is simulated under various scenarios. The model has two functional degree-of-freedom, which result from the modified universal joint utilized to formulate the ankle joint complex [18]. For the application of the RoM methodology, the modified universal joint can be thought of as two separate revolute joints, in which the RoM associated with each joint axis must be restricted independently. A detailed description of the application of the RoM methodology to the ankle joint complex of the human foot is provided, including the definition of the moving and reference bodies, the joint's local reference frames and circumduction cones, the estimation of the longitude and latitude, the calculation of the maximum latitude using the elliptical approach and

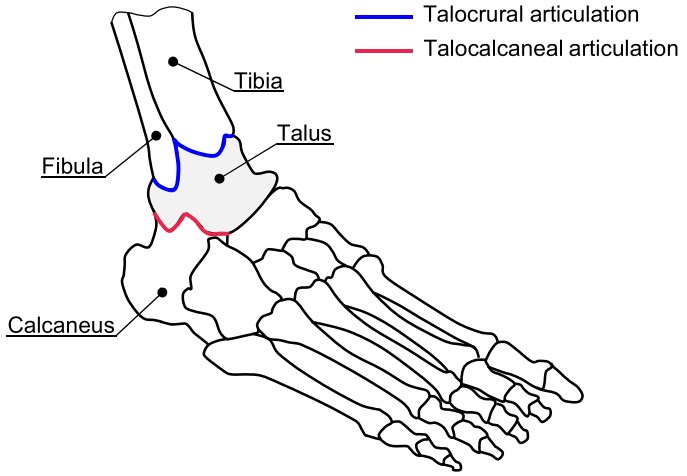

Fig. 1. Schematic representation of the ankle joint complex of the human foot.

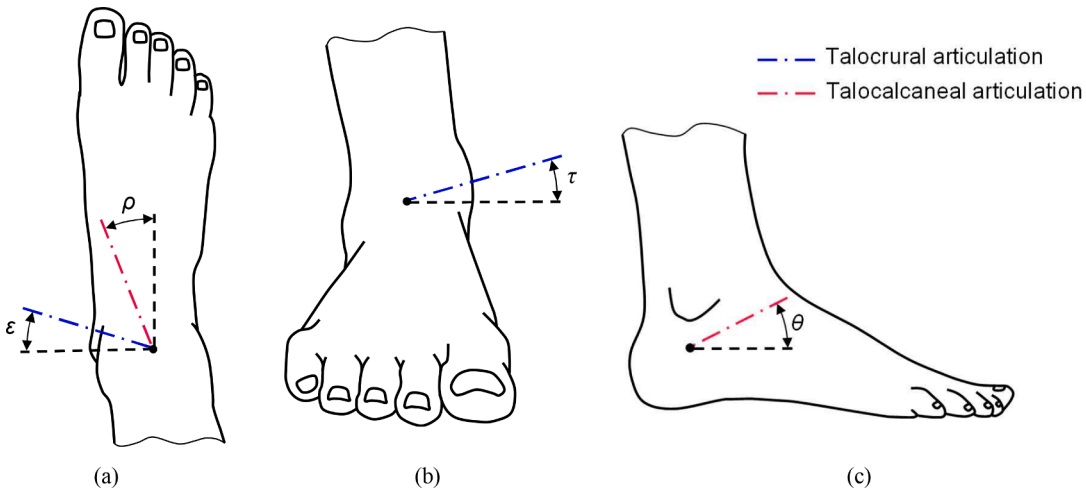

Fig. 2. Orientation of the talocrural and talocalcaneal axes in the (a) transverse, (b) frontal and (c) sagittal planes.

the transfer of forces and moments to the connected bodies.

The remaining of this article is organized as follows. A short explanation of the concepts of spatial multibody dynamics is given in Section 2. Then, Section 3 presents a description of the biomechanical model considered in this work. The application of the methodology to restrict the RoM of the ankle joint complex is explained in detail in Section 4. In Section 5, the obtained results are presented and discussed. Finally, the present work ends with the concluding remarks described in Section 6.

2. Spatial multibody dynamics

The dynamic analysis of multibody systems relies on the development of mathematical models and on the implementation of computational procedures to simulate or analyze their motion. One of the most common methods to model multibody biomechanical systems is the Newton-Euler approach with absolute coordinates due to its simplicity and straightforward application to general-purpose codes [10,11,34–36]. Considering the Baumgarte stabilization method, the equations of motion of a general constrained multibody system can be written as [10]

$$\begin{bmatrix} \mathbf{M} & \mathbf{D}^{\mathrm{T}} \\ \mathbf{D} & \mathbf{0} \end{bmatrix} \begin{Bmatrix} \dot{\mathbf{v}} \\ \boldsymbol{\lambda} \end{Bmatrix} = \begin{Bmatrix} \mathbf{g} \\ \boldsymbol{\gamma} - 2\alpha\dot{\boldsymbol{\Phi}} - \beta^2\boldsymbol{\Phi} \end{Bmatrix} \tag{5}$$

in which $\mathbf{M}$ is the system mass matrix, $\mathbf{D}$ represents the Jacobian matrix of the kinematic constraint equations, $\dot{\mathbf{v}}$ denotes the vector containing the system accelerations, $\boldsymbol{\lambda}$ is the Lagrange multipliers vector associated with the reaction forces and moments on the

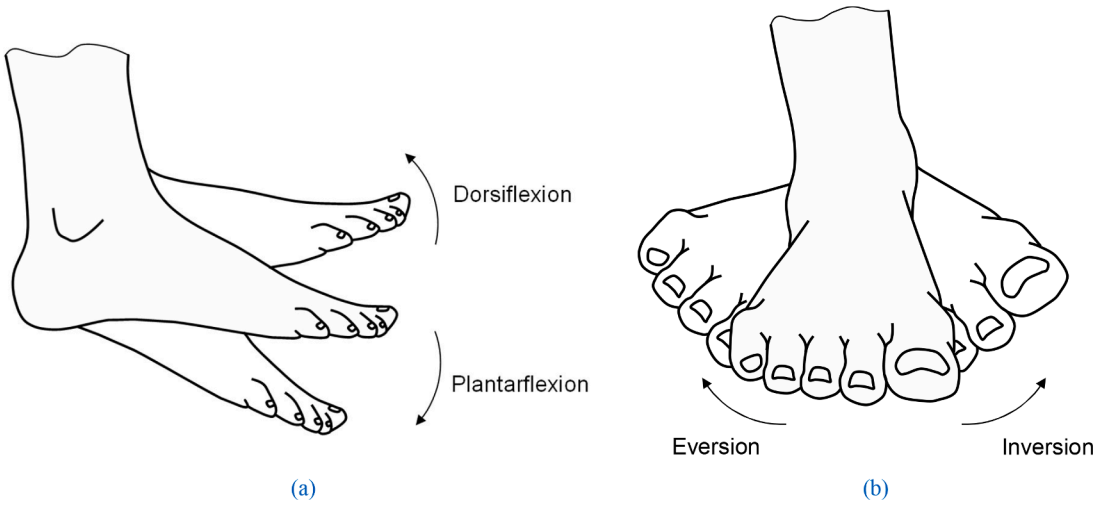

Fig. 3. Schematic representation of the movement of the human foot provided by the (a) talocrural and (b) talocalcaneal joints.

kinematic joints, $\mathbf{g}$ represents the generalized vector of externally applied forces and moments, and $\boldsymbol{\gamma}$ denotes the right-hand side vector of the acceleration constraint equations. Variables α and β are the feedback control parameters of the Baumgarte stabilization technique for velocity and position constraint violations, respectively, and are taken as positive constants. The terms $\boldsymbol{\Phi}$ and $\dot{\boldsymbol{\Phi}}$ represent the position and velocity constraint equations, respectively [10,37].

If the Baumgarte stabilization method is not taken into account in Eq. (5), the position, $\boldsymbol{\Phi}$, and velocity, $\dot{\boldsymbol{\Phi}}$, constraint equations are not explicitly included in the formulation, which may cause violation of those original constraints, unstable equations of motion and the divergence of the system response. These violations can also be associated with the integration procedure, selected time step, and/or inaccurate initial conditions [10,37].

3. Description of the biomechanical model

In this work, a three-dimensional biomechanical multibody model of the human leg, main foot and toes is considered for forward dynamics analysis. The model was established using an in-house code developed in Matlab named MUBODYNA [38], and it is composed of three rigid bodies, namely the toes, main foot, and leg, as depicted in Fig. 4. Anatomically, the leg represents the tibia and fibula bones, the main foot is composed of the tarsus and metatarsus, and the toes encompass the phalanges [18]. The three rigid bodies are kinematically connected to each other by means of one revolute joint, connecting the toes to the main foot and representing the metatarsophalangeal articulations, and one modified universal joint, incorporated with a massless link, connecting the main foot to the leg and representing the ankle joint complex [18,39]. In should be noted that the massless link represents the offset between the two articular axes of the ankle joint complex introduced by the talus bone. A fixed joint is considered at the center of mass of the leg, restraining the translation and rotation of this body. A constant angle kinematic constraint is utilized to lock the metatarsophalangeal joint angle using the following condition

$$\Phi \equiv \mathbf{s}_i^{\mathrm{T}}\mathbf{s}_j - \mathbf{s}_{i,0}^{\mathrm{T}}\mathbf{s}_{j,0} = 0 \tag{6}$$

where $\mathbf{s}_i$ and $\mathbf{s}_j$ are two vectors perpendicular to the joint axis that belong to bodies i and j, respectively, in global coordinates. The subscript '0′ denotes the coordinates of vectors $\mathbf{s}_i$ and $\mathbf{s}_j$ at the initial time step.

The biomechanical model has three degrees-of-freedom. However, since the metatarsophalangeal joint is subjected to the constant angle kinematic constraint of Eq. (6), in reality, the model has only two functional degrees-of-freedom, which result from the modified universal joint. The two degrees-of-freedom represent, respectively, the plantarflexion and dorsiflexion, and the inversion and eversion of the human foot, as discussed in Section 1.

A generic configuration of the biomechanical model, where the numbers of each body and their corresponding local coordinate systems are shown, is displayed in Fig. 4, and the corresponding initial positions are listed in Table 1. The local reference frames of the bodies are located at their center of mass (see Fig. 4) and are aligned with the principal axes of inertia. The locations of the center of mass of each body and all joints were assumed to be aligned with the midline of the foot, therefore, resulting in a null y-coordinate. The x, y, and z directions represent the anteroposterior, mediolateral and superoinferior directions in the three cardinal planes, respectively. The model is released from the initial configuration with null velocities and under the action of the gravitational force, which acts on the negative z-direction.

The dimensions and inertial properties of each body of the multibody system are listed in Table 2. The biomechanical model corresponds to a 71 kg and 1.77 m male subject [29]. The total foot length was considered to be 0.27 m [29] and the length of the massless link was taken as 0.0417 m [40].

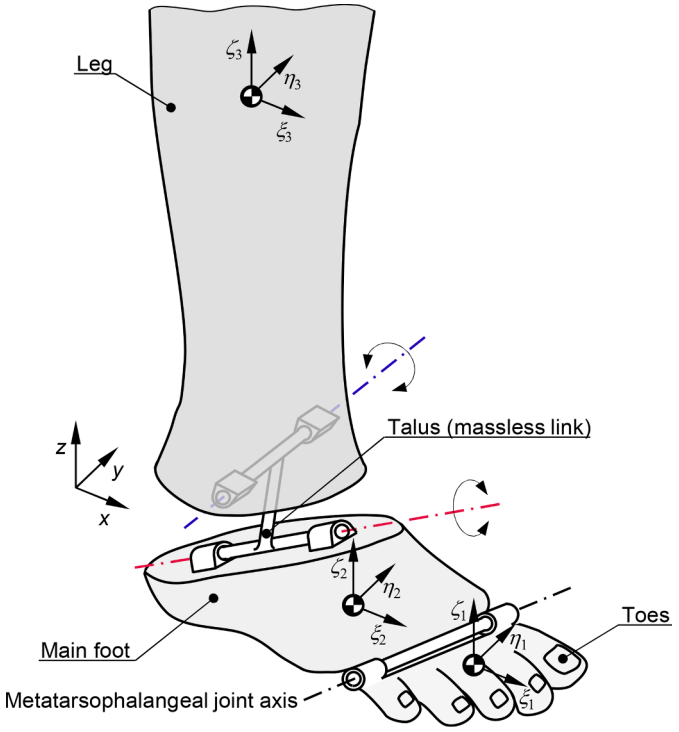

Fig. 4. Schematic representation of the biomechanical multibody model of the human leg, main foot and toes.

The location of the metatarsophalangeal, talocalcaneal and talocrural joints with respect to the local reference frames of the toes, main foot and leg can be consulted in Table 3.

The parameters utilized in the dynamic simulations and in the numerical methods required to solve the dynamics of the system are based on [18,23] and are presented in Table 4.

4. Application of the methodology

The methodology considered here to restrict the RoM of joints is based on the authors' previous work [23]. The interested reader is referred to [23] for a detailed explanation of the concepts and formulations utilized in this Section. In order to restrict the RoM of joints, the methodology utilizes joint resistance moments, which are applied to the connected bodies to mimic the dissipative and resistive behavior of the constituent materials and to prevent unacceptable configurations of those bodies [19,23,41–43]. Two terms contribute to the joint resistance moments, $\mathbf{m}_h^{\mathrm{r}}$, as

$$\mathbf{m}_h^{\mathrm{r}} = \mathbf{m}_h^{\mathrm{d}} + \mathbf{m}_h^{\mathrm{mr}} \tag{7}$$

in which $\mathbf{m}_h^{\mathrm{d}}$ is the joint dissipative moment vector, and $\mathbf{m}_h^{\mathrm{mr}}$ represents the joint motion-restricting moment vector. The subscript h denotes the joint index.

A joint connects two bodies whose relative motion has to be restricted, and, in this methodology, they are referred to as the reference and moving bodies. The moving body is the one whose RoM is intended to be restricted, and the reference body is the one that allows the definition of the limits inside which the moving body can move without exceeding the RoM of the joint. Since the joint resistance moments represent an action-reaction pair, the results obtained using Eq. (7) are applied on the moving body and their symmetrical counterparts are applied on the reference body. In the multibody systems methodology, these moments are integrated in vector $\mathbf{g}$ of Eq. (5) [10,11,23,43].

The metatarsophalangeal joint angle of the biomechanical model described in Section 3 is locked using Eq. (6), and, thus, the corresponding RoM is not restricted. In this sense, only the talocrural and talocalcaneal joints, which are formulated using a modified

Table 1
Initial positions for the biomechanical multibody model [18,29].

Body (nr.)	x [m]	y [m]	z [m]	e_0	e_1	e_2	e_3
Toes (1)	0.2177	0.0000	0.0367	1.0000	0.0000	0.0000	0.0000
Main Foot (2)	0.0907	0.0000	0.0562	1.0000	0.0000	0.0000	0.0000
Leg (3)	0.0544	0.0000	0.3513	1.0000	0.0000	0.0000	0.0000

Table 2
. Geometric length and inertial properties of the bodies of the biomechanical multibody model [18,29].

Body (nr.)	Length [m]	Mass [kg]	Moment of inertia [kg·m^2]		
			$I_{\xi\xi}$	$I_{\eta\eta}$	$I_{\zeta\zeta}$
Toes (1)	0.0797	0.2051	0.0001003	0.0001003	0.0002006
Main Foot (2)	0.1903	1.2000	0.0013818	0.0038337	0.0037110
Leg (3)	0.4300	3.5100	0.0477209	0.0483791	0.0048000

Table 3
. Location of the metatarsophalangeal, talocalcaneal and talocrural joints in local coordinates.

Joint	Body (nr.)	ξ [m]	η [m]	ζ [m]
Metatarsophalangeal	Toes (1)	−0.0274	0.0000	−0.0185
Metatarsophalangeal	Main Foot (2)	0.0996	0.0000	−0.0380
Talocalcaneal	Main Foot (2)	−0.0363	0.0000	0.0096
Talocrural	Leg (3)	0.0000	0.0000	−0.2438

Table 4
Parameters utilized in the dynamic simulation of the biomechanical multibody model.

Dynamic Simulation Data			
Baumgarte coefficient - α	5	Reporting time step	0.00001 s
Baumgarte coefficient - β	5	Relative and absolute integration tolerances	10^{-10}
Integration algorithm	ode15s	Simulation time	5 s

universal joint, are subjected to the joint resistance moments of Eq. (7). For the application of the RoM methodology, the modified universal joint can be thought of as two separate revolute joints, which means that the RoM associated with each joint axis must be restricted independently.

The joint motion-restricting moment is formulated as a non-linear elastic element, which is null during admissible joint motions and varies from zero to a maximum value whenever an unacceptable configuration of the moving body is detected. The methodology considers that the acceptable configuration of a joint is established by the circumduction cone, which is a three-dimensional surface inside which any configuration of the joint is physiologically acceptable [23,43,44]. The circumduction cone can be established for any joint with rotational degrees-of-freedom, independently of its number of degrees-of-freedom. For instance, for a revolute joint, some sections of the cone are not reached by the moving body due to the intrinsic kinematic structure of this type of joint. The circumduction cone is characterized by defining the axes of the joint's local coordinate system using the local coordinate system of the reference body. For the talocrural and talocalcaneal joints, the reference bodies are the leg and the main foot, respectively. In the cones illustrated in Fig. 5, the unit vectors defining the axes ξ, η and ζ of the joint's local coordinate system are established as

$$\mathbf{u}'_{\xi,h} = \{\cos\varepsilon \quad -\sin\varepsilon \quad 0\}^{\mathrm{T}}$$

$$\mathbf{u}'_{\eta,h} = \{-\sin\varepsilon\cos\tau_{re} \quad -\cos\varepsilon\cos\tau_{re} \quad -\sin\tau_{re}\}^{\mathrm{T}}$$

$$\mathbf{u}'_{\zeta,h} = \{\sin\varepsilon\sin\tau_{re} \quad \cos\varepsilon\sin\tau_{re} \quad -\cos\tau_{re}\}^{\mathrm{T}}$$

for the talocrural joint and as

$$\mathbf{u}'_{\xi,h} = \{\cos\rho\cos\theta_{re} \quad \sin\rho\cos\theta_{re} \quad \sin\theta_{re}\}^{\mathrm{T}}$$

$$\mathbf{u}'_{\eta,h} = \{-\sin\rho \quad \cos\rho \quad 0\}^{\mathrm{T}}$$

$$\mathbf{u}'_{\zeta,h} = \{-\cos\rho\sin\theta_{re} \quad -\sin\rho\sin\theta_{re} \quad \cos\theta_{re}\}^{\mathrm{T}}$$

for the talocalcaneal joint. The symbol $(')$ represents the components of vector $\mathbf{u}$ in the body's local coordinate system [34].

After the definition of the joint's local coordinate system, a unit vector, $\mathbf{u}_{\mathrm{r},h}$, which allows to identify, in every configuration, the orientation of the moving body in the joint's local coordinate system, with the exception of the internal rotation, must be established. For the talocrural and talocalcaneal joints, the moving bodies are the main foot and the leg, respectively. In a modified universal joint, vector $\mathbf{u}_{\mathrm{r},h}$ is the massless link. However, in order to ensure that the RoM associated with each joint is correctly restricted, vector $\mathbf{u}_{\mathrm{r},h,\mathrm{p}}$, which denotes the projection of the massless link onto the plane perpendicular to the axis of the joint whose RoM is intended to be restricted (see Figs. 5 and 6), must be considered. Vector $\mathbf{u}_{\mathrm{r},h,\mathrm{p}}$ is calculated using the following condition (see Fig. 6)

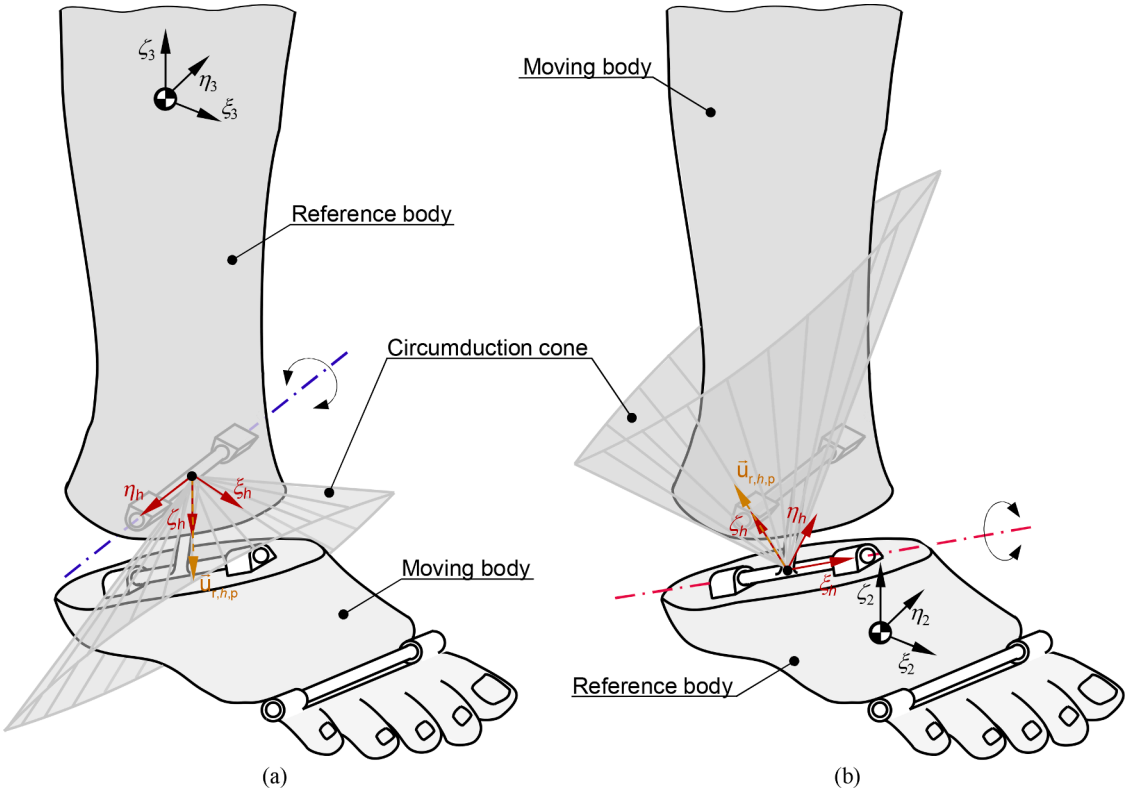

Fig. 5. Schematic representation of the circumduction cones for the (a) talocrural and (b) talocalcaneal joints. The talocrural, and talocalcaneal joint axes are highlighted in blue and red, respectively.

$$\mathbf{u}_{\mathrm{r},h,\mathrm{p}} = \frac{\mathbf{u}_{\mathrm{r},h} - \left(\mathbf{u}_{\mathrm{r},h}^{\mathrm{T}}\mathbf{s}_i\right)\mathbf{s}_i}{\| \mathbf{u}_{\mathrm{r},h} - \left(\mathbf{u}_{\mathrm{r},h}^{\mathrm{T}}\mathbf{s}_i\right)\mathbf{s}_i \|} \tag{8}$$

where $\mathbf{u}_{\mathrm{r},h,\mathrm{p}}$ is the projection of vector $\mathbf{u}_{\mathrm{r},h}$, and $\mathbf{s}_i$ represents a unit vector along the joint axis given either by Eqs. (3) or (4) (see Fig. 6). Since the massless link does not belong to any particular body, vector $\mathbf{u}_{\mathrm{r},h}$ does not have constant coordinates in any of the local coordinate systems. It is important to note that the definition of both the unit vector $\mathbf{u}_{\mathrm{r},h}$ and the circumduction cone must ensure that, in its initial state, the joint does not hold an unacceptable configuration.

Fig. 6 provides a schematic representation of two bodies i and j connected by a modified universal joint, with joint axis $\mathbf{s}_i$ and $\mathbf{s}_j$, respectively. An example is given for the $\mathbf{s}_i$ joint axis. The massless link, vector $\mathbf{u}_{\mathrm{r},h}$, and the projection of the massless link onto the plane perpendicular to the $\mathbf{s}_i$ joint axis, vector $\mathbf{u}_{\mathrm{r},h,\mathrm{p}}$, are illustrated.

The moving body is in an unacceptable configuration whenever it is located outside the circumduction cone. In these circumstances, a joint motion-restricting moment must be applied to reposition the moving body into an acceptable configuration. In order to determine whether the actual position of the moving body is inside (acceptable configuration) or outside (unacceptable configuration) the circumduction cone, the longitude, ψ_h, and latitude, σ_h, of the unit vector $\mathbf{u}_{\mathrm{r},h,\mathrm{p}}$ expressed in the joint's local coordinate system must be determined [23]. The longitude, ψ_h, is established by the joint's local ξ_h axis and the projection of vector $\mathbf{u}_{\mathrm{r},h,}$ in the plane $\xi_h\eta_h$ of the joint's local coordinate system (see Fig. 7a). The longitude is calculated as [23]

$$\psi_h = \arctan\left(\frac{u''_{\mathrm{r},h,\mathrm{p},\eta}}{u''_{\mathrm{r},h,\mathrm{p},\xi}}\right) \tag{9}$$

where $(''$) represents the components of vector $\mathbf{u}_{\mathrm{r},h,\mathrm{p}}$ expressed in the joint's local coordinate system. It must be highlighted that, when dealing with revolute joints, as in the present case, the longitude can only assume values of 0° or 180°, or 90° or 270° in order to fulfill the kinematic constraints.

The latitude, σ_h, is established by the joint's local unit vector $\mathbf{u}_{\zeta,h}$ and the unit vector $\mathbf{u}_{\mathrm{r},h,\mathrm{p}}$, as illustrated in Fig. 7b. Thus, the latitude can be calculated using the following condition [23]

$$\sigma_h = \arccos\left(\mathbf{u}''^{T}_{\mathrm{r},h,\mathrm{p}}\,\mathbf{u}''_{\zeta,h}\right) \tag{10}$$

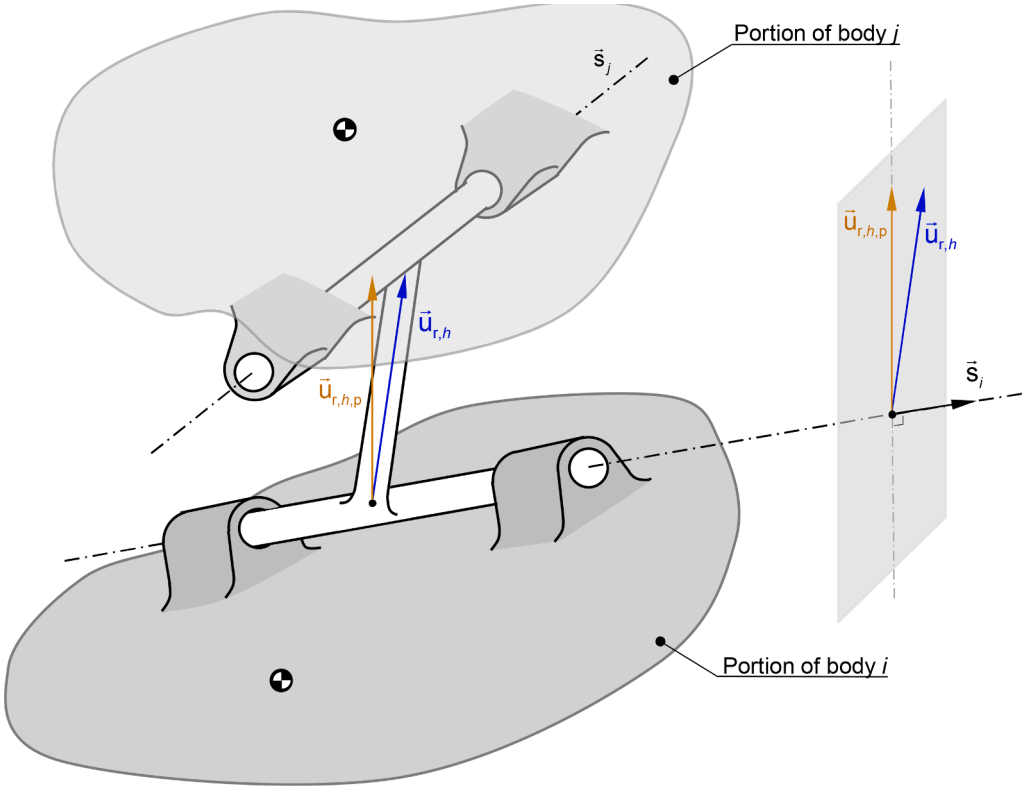

Fig. 6. Schematic representation of representation of two bodies i and j connected by a modified universal joint, with joint axis $\mathbf{s}_i$ and $\mathbf{s}_j$, respectively. Vectors $\mathbf{u}_{r,h}$ and $\mathbf{u}_{r,h,p}$ are illustrated.

The reference frame for each joint of the ankle may be defined such that the vector $\mathbf{u}_{\zeta,h}$ has the same orientation as vector $\mathbf{u}_{r,h,p}$ at the initial configuration (see Fig. 5). Thus, in this situation, the latitude is zero.

At this stage, all the necessary ingredients to construct the circumduction cone have been described. The cone is defined by specifying the maximum allowable latitude, $\sigma_{h,max}$, for certain values of longitude, ψ_h. Then, an interpolation function is created in order to estimate the maximum allowable latitude corresponding to any value of longitude. In this work, the maximum latitude for

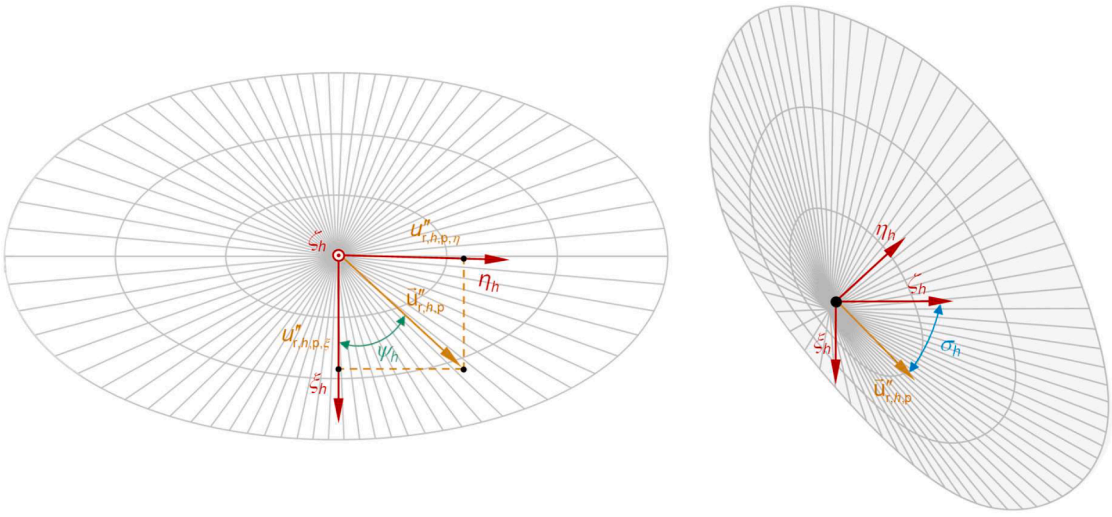

(a) (b)

Fig. 7. Schematic representation of the (a) longitude, ψ_h, and (b) latitude, σ_h, for the calculation of the joint motion-restricting moment. The longitude is defined in the plane $\xi_h\eta_h$ of the joint's local coordinate system (top view of the circumduction cone).

talocrural dorsiflexion and plantarflexion is considered to be 20° and 35°, respectively. In turn, talocalcaneal maximum inversion and eversion are defined as 35° and 25°, respectively [45]. Since, in a modified universal joint, the restriction of the RoM is achieved by considering two separate revolute joints, two circumduction cones must be constructed. The longitude was defined, for both joints, as

$$\boldsymbol{\psi}_h = \{\, 0^\circ \quad 90^\circ \quad 180^\circ \quad 270^\circ \quad 360^\circ \,\}$$

The maximum latitude for the talocrural and talocalcaneal joints was defined, respectively, as

$\boldsymbol{\sigma}_{h,\max} = \{\, 20^\circ \quad 1^\circ \quad 35^\circ \quad 1^\circ \quad 20^\circ \,\}$ and $\boldsymbol{\sigma}_{h,\max} = \{\, 1^\circ \quad 25^\circ \quad 1^\circ \quad 35^\circ \quad 1^\circ \,\}$

The differences in the maximum latitude are associated with the definition of the joint's local coordinate system for each joint (see Fig. 5). Furthermore, a value of 1° is utilized as a tolerance in the locations of the circumduction cone that are not reached due to the kinematic structure of a revolute joint. As observed in the above conditions, the maximum allowable latitude for both the talocrural and talocalcaneal joints is defined for longitude values that coincide with the limits of the four main quadrants, namely 0°, 90°, 180°, 270° and 360° (see Fig. 8). Thus, the maximum allowable latitude for any longitude is calculated using the elliptical approach, which treats each quarter of the ellipse independently, as [23]

$$\sigma_{h,\max}(\psi_h) = \sqrt{\frac{b^2}{\tan^2(\psi_h) + \frac{b^2}{a^2}}\left(1 - \frac{b^2}{a^2}\right) + b^2} \tag{11}$$

where a and b are constants representing the length of the semi-axes of the ellipse for a given quarter and, in this methodology, denote the defined maximum latitude values (see Fig. 8).

The joint motion-restricting moment corresponds to a third-degree polynomial function with the behavior depicted in Fig. 9, and it is expressed as [23,43,46]

$$\mathbf{m}_h^{\mathrm{mr}} = \begin{cases} \mathbf{0} & \text{if} \quad \sigma_h \le \sigma_{h,\max} \\ m_{\mathrm{p},h}\left[3\left(\dfrac{\kappa}{\Delta\sigma_h}\right)^2 - 2\left(\dfrac{\kappa}{\Delta\sigma_h}\right)^3\right]\tilde{\mathbf{u}}_{\mathrm{r},h,\mathrm{p}}\mathbf{n} & \text{if} \quad \sigma_{h,\max} < \sigma_h \text{and} \kappa \le \Delta\sigma_h \\ m_{\mathrm{p},h}\tilde{\mathbf{u}}_{\mathrm{r},h,\mathrm{p}}\mathbf{n} & \text{if} \quad \kappa > \Delta\sigma_h \end{cases} \tag{12}$$

where $m_{\mathrm{p},h}$ is the magnitude of the maximum penalty moment applied to restrict the joint's motion, $\Delta\sigma_h$ corresponds to the angular range between the cone limit and the maximum moment application, allowing to adjust the joint's stiffness, κ denotes the relative angular motion between the moving body and the limits of the circumduction cone and $\mathbf{n}$ represents the direction normal to the surface of the circumduction cone for the corresponding value of $\sigma_{h,\max}$ [23]. Values of 11.5° and 226 N·m were considered for $\Delta\sigma_h$ and $m_{\mathrm{p},h}$, respectively, and were both retrieved from [43,46]. The symbol (~) represents the skew-symmetric matrix associated with that vector [34].

Eq. (12) can be substituted by others existing in the literature, such as the ones given in the works of Yamaguchi [19] and Nasr et al. [47], or can be obtained by experimental testing, while keeping unchanged the remaining methodology described in the previous paragraphs.

It is important to note that, in the following formulation, the reference and moving bodies are denoted as bodies i and j, respectively. When the moving body is located in an unacceptable configuration, the joint motion-restricting moment, calculated utilizing Eq. (12), must be directly applied to the reference body, $\mathbf{m}_{h,i}^{\mathrm{mr}}$, and to the massless link, $\mathbf{m}_{h,\mathrm{massless}}^{\mathrm{mr}}$. However, since the massless link is a vector connecting two bodies and it does not belong to any of them, the joint motion-restricting moment is not directly applied to the moving body. Thus, the moment applied to the massless link, $\mathbf{m}_{h,\mathrm{massless}}^{\mathrm{mr}}$, must be transferred to both the moving and the reference

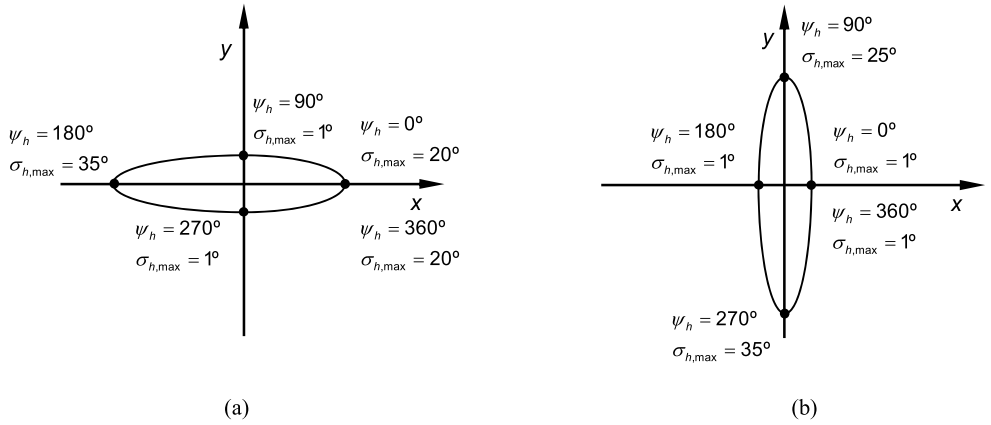

Fig. 8. Schematic representation of the top view of the circumduction cone with the longitude and maximum latitude specified for the **(a)** talocrural and **(b)** talocalcaneal joints.

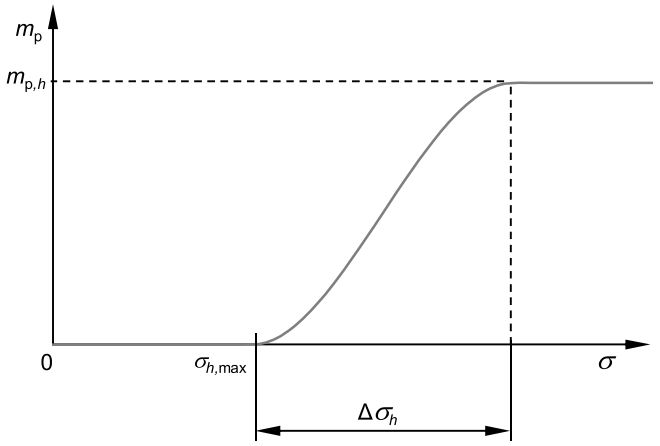

Fig. 9. Graphical representation of the third-degree polynomial function for the joint motion-restricting moment.

bodies. A schematic representation of the force and moment transfer phenomenon for the modified universal joint is displayed in Fig. 10.

The joint motion-restricting moment applied to the massless link, $\mathbf{m}^{mr}_{h,massless}$, generates a force on the reference body, $\mathbf{f}_{h,i}$, which is calculated as

$$\mathbf{f}_{h,i} = \left(\frac{\widetilde{\mathbf{u}}_{r,h,p} \mathbf{m}^{mr}_{h,massless}}{\| \mathbf{u}_{r,h,p} \| \| \mathbf{m}^{mr}_{h,massless} \|} \right) f_{h,i} \tag{13}$$

in which $f_{h,i}$ is the force magnitude evaluated as

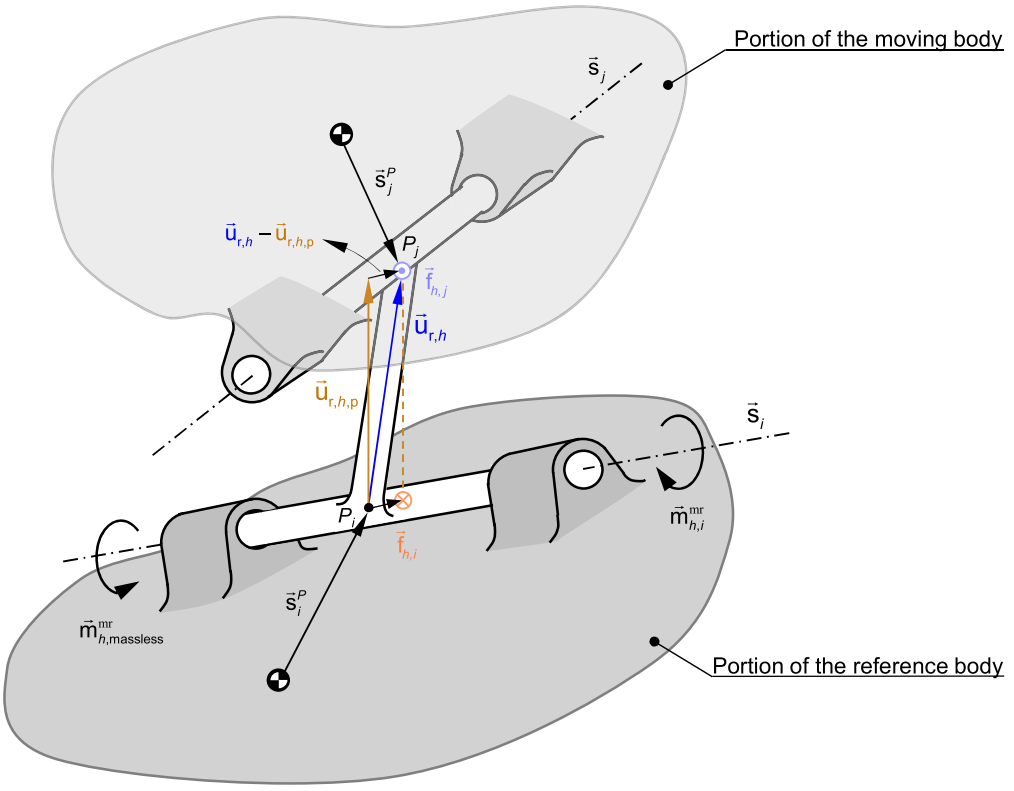

Fig. 10. Schematic representation of the force and moment transfer phenomenon in a modified universal joint.

$$f_{h,i} = \frac{\| \mathbf{m}^{\mathrm{mr}}_{h,\mathrm{massless}} \|}{\| \mathbf{u}_{\mathrm{r},h,\mathrm{p}} \|} \tag{14}$$

Force $\mathbf{f}_{h,i}$ generates a moment on the reference body, which is established as

$$\mathbf{m}_{h,i} = \widetilde{\mathbf{l}}_{h,i} \mathbf{f}_{h,i} \tag{15}$$

where $\mathbf{l}_{h,i}$ is the moment lever arm from the point of force application to the center of mass of the reference body, which, as shown in Fig. 10, can be calculated as

$$\mathbf{l}_{h,i} = \mathbf{s}^{P}_{i} + \left(\mathbf{u}_{\mathrm{r},h} - \mathbf{u}_{\mathrm{r},h,\mathrm{p}} \right) \tag{16}$$

in which $\mathbf{s}^{P}_{i}$ is the global position vector of point P_i located on the reference body with respect to the body's local coordinate system.

The force applied to the reference body, $\mathbf{f}_{h,i}$, must be applied to the moving body with opposite direction, $\mathbf{f}_{h,j}$, as

$$\mathbf{f}_{h,j} = -\mathbf{f}_{h,i} \tag{17}$$

The force $\mathbf{f}_{h,j}$ produces a moment because its application point is displaced from the center of mass of the moving body as

$$\mathbf{m}_{h,j} = \widetilde{\mathbf{s}}^{P}_{j} \mathbf{f}_{h,j} \tag{18}$$

In biomechanical models, the joint dissipative moment allows to simulate the dissipative behavior of the tissues that exist around human articulations, such as muscles, ligaments, or cartilage [19,42,48]. The joint dissipative moment is formulated using a viscous torsional damper as [43]

$$\mathbf{m}^{\mathrm{d}}_{h} = -j_h \boldsymbol{\omega}_h \tag{19}$$

in which j_h is the rotational damping coefficient of the joint h and $\boldsymbol{\omega}_h$ denotes the joint h angular velocity vector. The joint dissipative moment given by Eq. (19) is associated with the energy loss due to the viscoelasticity of the tissues existing around human articulations. In this work, the damping coefficient for the ankle joint complex, j_h, was obtained by multiplying the total mass of the subject by the normalized value 0.008 N·m·s/kg [49,50]. Thus, a value of 0.5680 N·m·s was utilized. Since two circumduction cones are considered for the application of the RoM methodology, half of this value is applied to each cone (0.2840 N·m·s). Due to consideration of the massless link in a modified universal joint, the angular velocity of each joint is calculated based on the velocities of the adjacent bodies as (see Fig. 11)

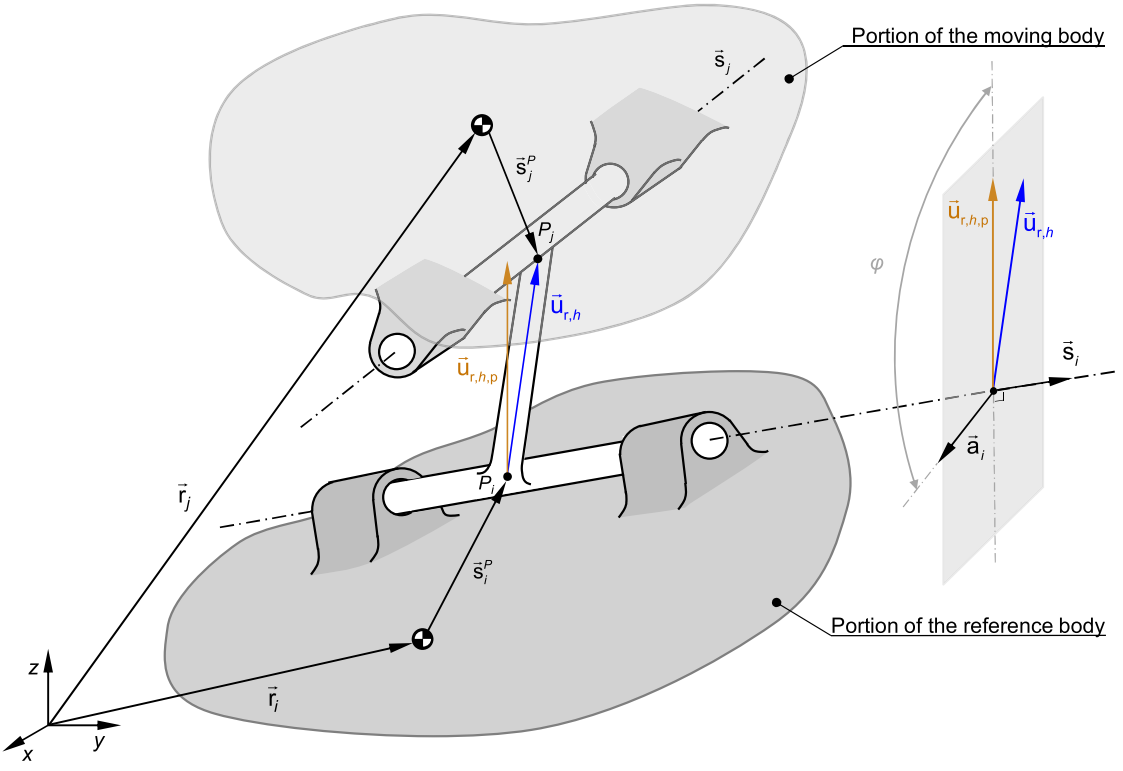

Fig. 11. Schematic representation of the vectors utilized to calculate the angular velocity of each joint of a modified universal joint.

$$\boldsymbol{\omega}_h = -\frac{1}{\| \mathbf{u}_{\mathrm{r},h,\mathrm{p}} \| \sin\varphi} \Big(\mathbf{a}_i^{\mathrm{T}} \left(\mathbf{s}_i \mathbf{s}_i^{\mathrm{T}} - \mathbf{I} \right) \dot{\mathbf{r}}_i + \Big(- \mathbf{u}_{\mathrm{r},h,\mathrm{p}}^{\mathrm{T}} \tilde{\mathbf{a}}_i + \mathbf{a}_i^{\mathrm{T}} \left(\tilde{\mathbf{s}}_i^{P} - \mathbf{s}_i \mathbf{s}_i^{\mathrm{T}} \tilde{\mathbf{s}}_i^{P} + \mathbf{s}_i \mathbf{u}_{\mathrm{r},h}^{\mathrm{T}} \tilde{\mathbf{s}}_i + \mathbf{u}_{\mathrm{r},h}^{\mathrm{T}} \mathbf{s}_i \tilde{\mathbf{s}}_i \right) \Big) \boldsymbol{\omega}_i + \mathbf{a}_i^{\mathrm{T}} \left(\mathbf{I} - \mathbf{s}_i \mathbf{s}_i^{\mathrm{T}} \right) \dot{\mathbf{r}}_j + \mathbf{a}_i^{\mathrm{T}} \left(\mathbf{s}_i \mathbf{s}_i^{\mathrm{T}} \tilde{\mathbf{s}}_j^{P} - \tilde{\mathbf{s}}_j^{P} \right) \boldsymbol{\omega}_j \Big) \tag{20}$$

in which $\mathbf{a}_i$ represents one arbitrary unit vector perpendicular to the $\mathbf{s}_i$ joint axis, φ is the joint angle, which is measured between vectors $\mathbf{a}_i$ and $\mathbf{u}_{\mathrm{r},h,\mathrm{p}}$, as represented in Fig. 11 for the case of the talocalcaneal joint, $\mathbf{s}_k^P$ ($k = i, j$) is the global position vector of point P, the insertion of the massless link, located on body k with respect to the body's local coordinate system, $\mathbf{I}$ denotes the identity matrix, $\dot{\mathbf{r}}_k$ denotes the velocity vector of the center of mass of body k described in global coordinates, and $\boldsymbol{\omega}_k$ denotes the angular velocity vector of body k.

5. Results and discussion

This section presents and discusses the results of the application of the proposed methodology to restrict the RoM of the ankle joint complex of the biomechanical model. In what follows, the results of three analyses are shown. In the first analysis, the biomechanical model is released from the initial position, with null velocities, and under the action of the gravitational force only. The second and third analyses are similar to the first case but include the joint resistance moments to restrict the RoM of the talocrural and talocalcaneal joints without and with energy dissipation, respectively.

The trajectory of the center of mass of the main foot segment throughout the simulation time in the three cardinal planes can be observed in Fig. 12. The initial conditions defined for the biomechanical model, in which, at the initial configuration, the foot is horizontal with respect to the ground, prevent the talocrural joint from reaching its maximum latitude for dorsiflexion. However, for the talocalcaneal joint, no limitation is imposed by the initial conditions. By analyzing Fig. 12, significant differences in the trajectory of the center of mass of the main foot segment are observed for all analyses and for all three cardinal planes. For talocrural plantarflexion, the amplitude of movement of the center of mass is higher when the RoM methodology is not considered. In turn, when the RoM methodology is applied, with or without energy dissipation, the amplitude of movement is significantly decreased. This fact can be observed in the anteroposterior (x-direction) and superoinferior (z-direction) directions (see Fig. 12). The maximum latitude for eversion is not reached for the talocalcaneal joint in the case where the RoM methodology is not applied. This can be concluded by the fact that, in Fig. 12b and c, the blue plot reaches higher position values than the grey plot in the lateral direction (negative y). For talocalcaneal inversion (medial direction, positive y), the model exceeded the maximum latitude in the first analysis. This occurrence was corrected with the application of the RoM methodology. It is important to note that, for the case of RoM methodology application without energy dissipation, the trajectory of the center of mass of the main foot is less smooth due to the successive joint resistance moment applications to prevent the RoM from being exceeded, which impose successive changes of direction. With the addition of energy dissipation to the system, a smoother behavior of the trajectory of the center of mass of the main foot segment is observed in all cardinal planes. Overall, energy dissipation helps to stabilize the system.

Fig. 13 presents several snapshots of the movement of the biomechanical multibody model for the first second of simulation in order to provide a comparison of the amplitude of motion and type of movement between the three cases tested in Fig. 12.

In order to examine whether the maximum latitude for plantarflexion, eversion and inversion is properly restricted with the application of the proposed RoM methodology, the evolution of the latitude as a function of the longitude for the talocrural and talocalcaneal joints is depicted in Fig. 14. When the RoM methodology is not considered, the model exceeded the maximum latitude for plantarflexion since a latitude of almost 90° is reached for ψ_h=180°, as opposed to a maximum latitude of 37° and 35° observed when the RoM methodology is considered without and with energy dissipation, respectively (see Fig. 14a and c). When energy dissipation is not considered, the latitude exceeds the maximum allowable latitude by 2° because a value of 11.5° was set for parameter $\Delta\sigma_h$, which allows to adjust the joint stiffness. Furthermore, the maximum latitude for dorsiflexion is not reached (ψ_h=0°). It must be emphasized that, in the present application example, when the RoM methodology is taken into account with energy dissipation, the model reaches the equilibrium position in the maximum latitude for plantarflexion, since the gravitational force tends to lead the foot outwards its normal RoM. For the talocalcaneal joint, as concluded previously in Fig. 12, when the RoM is not considered, the maximum latitude for eversion is not reached (ψ_h=270°), as opposed to the maximum latitude for inversion (ψ_h=90°). In the cases in which the RoM methodology is applied, the maximum latitude for both of these movements is adequately restricted to the respective defined values, considering the parameter $\Delta\sigma_h$ (see Fig. 14b and d).

Fig. 15 shows the evolution of the joint dissipative moment and the joint motion-restricting moment for both the talocrural and talocalcaneal joints throughout the simulation time. Since none of these moments are applied to the model in both joints when the RoM methodology is not considered, this case in not depicted in Fig. 15. When the RoM methodology is applied without energy dissipation, only the joint motion-restricting moment is acting on the model. This situation is expected since, with no energy dissipation, the maximum latitude for plantarflexion, inversion and eversion are reached, as discussed above (see Figs. 12 and 14). The joint dissipative moment is only applied when energy dissipation is considered in the RoM methodology and its curve and magnitude differ for both joints (see Fig. 15a and b), which is sound because the angular velocity calculated using Eq. (20) is different. However, it is important to note that the dissipative moment applied in the talocrural joint is nearly three times higher than that applied in the talocalcaneal joint. For the talocalcaneal joint, when energy dissipation is considered, only the joint dissipative moment is acting on the model, since the maximum latitude for inversion and eversion is not exceeded (see Fig. 15b and d). However, when the RoM is considered with energy dissipation, both moments are acting on the talocrural joint (see Fig. 15a and c). This phenomenon occurs because the maximum latitude for plantarflexion is reached at around 0.43 s of simulation, as observed in Fig. 14a for ψ_h=180°. Since the joint

Sagittal plane

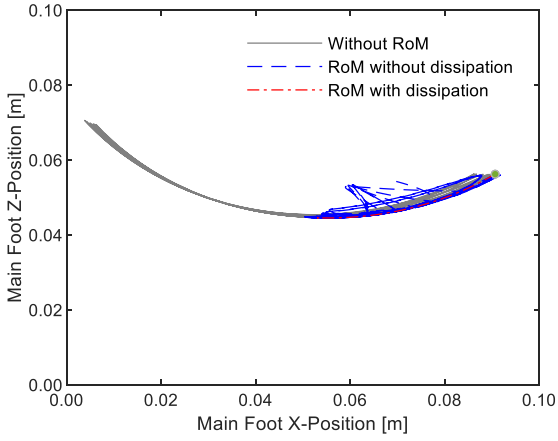

(a)

Transverse plane

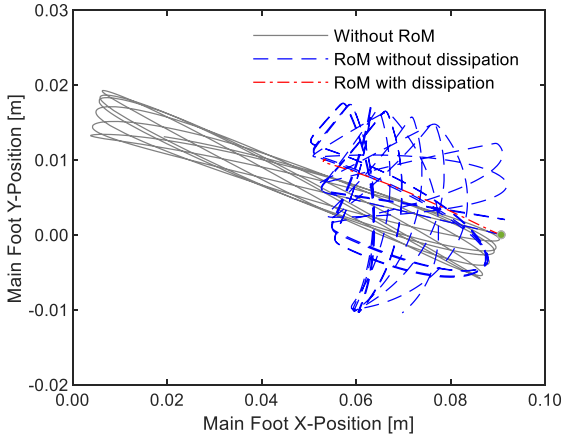

(b)

Frontal plane

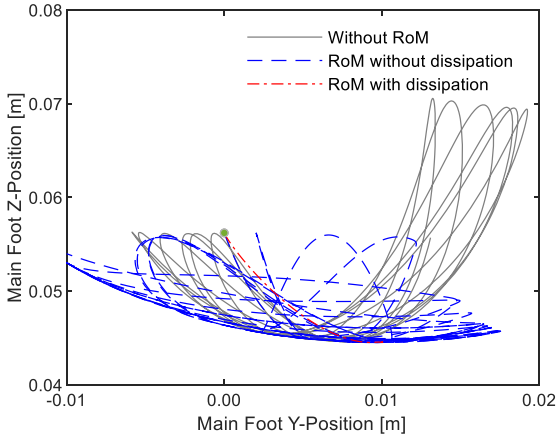

(c)

Fig. 12. Trajectory of the center of mass of the main foot in the (a) sagittal, (b) transverse and (c) frontal planes. The green marker represents the initial position of the center of mass of the main foot. The *x*, *y*, and *z* directions correspond to the anteroposterior, mediolateral and superoinferior directions in the three cardinal planes, respectively.

dissipative moment is acting on the model, the relative velocity of the bodies decreases during the simulation. Thus, in the first time the maximum latitude for talocrural plantarflexion is detected, the magnitude of the joint motion-restricting moment is maximum and decreases in subsequent detections, before stabilizing around 0.14 N·m (see Fig. 15c). After stabilization, the model remains in the same configuration for the remainder of the simulation, and, therefore, a constant magnitude of joint motion-restricting moment is applied to prevent the plantarflexion RoM from being exceeded. In general, the application of the joint motion-restricting moment is responsible for the discontinuities observed in the curves of the joint dissipative moment in plots of Fig. 15a and b. Finally, the magnitude of the joint motion-restricting moment for both joints is much higher than that observed for the joint dissipative moment (see Fig. 15). However, in general, the joint motion-restricting moment is applied in a very short period of time, as opposed to the joint dissipative moment.

Since the required calculations for the three compared scenarios do not differ significantly, the computational cost of the biomechanical model was evaluated through the number of function evaluations, and it is depicted in Fig. 16. When energy dissipation was considered in the RoM methodology and when the 5-second simulation was utilized to evaluate the computational cost of the biomechanical multibody model, the system showed numerical issues after it was fully dampened. These issues are directly associated with the numerical error that arises from the integration process and that does not allow to obtain exactly null velocities and, thus, fully stop the motion of the bodies. In turn, very low velocities are calculated using Eq. (5), which provoke variations in the position and velocity of the bodies of the biomechanical model, leading to a continuous application of a joint dissipative moment to the system. The

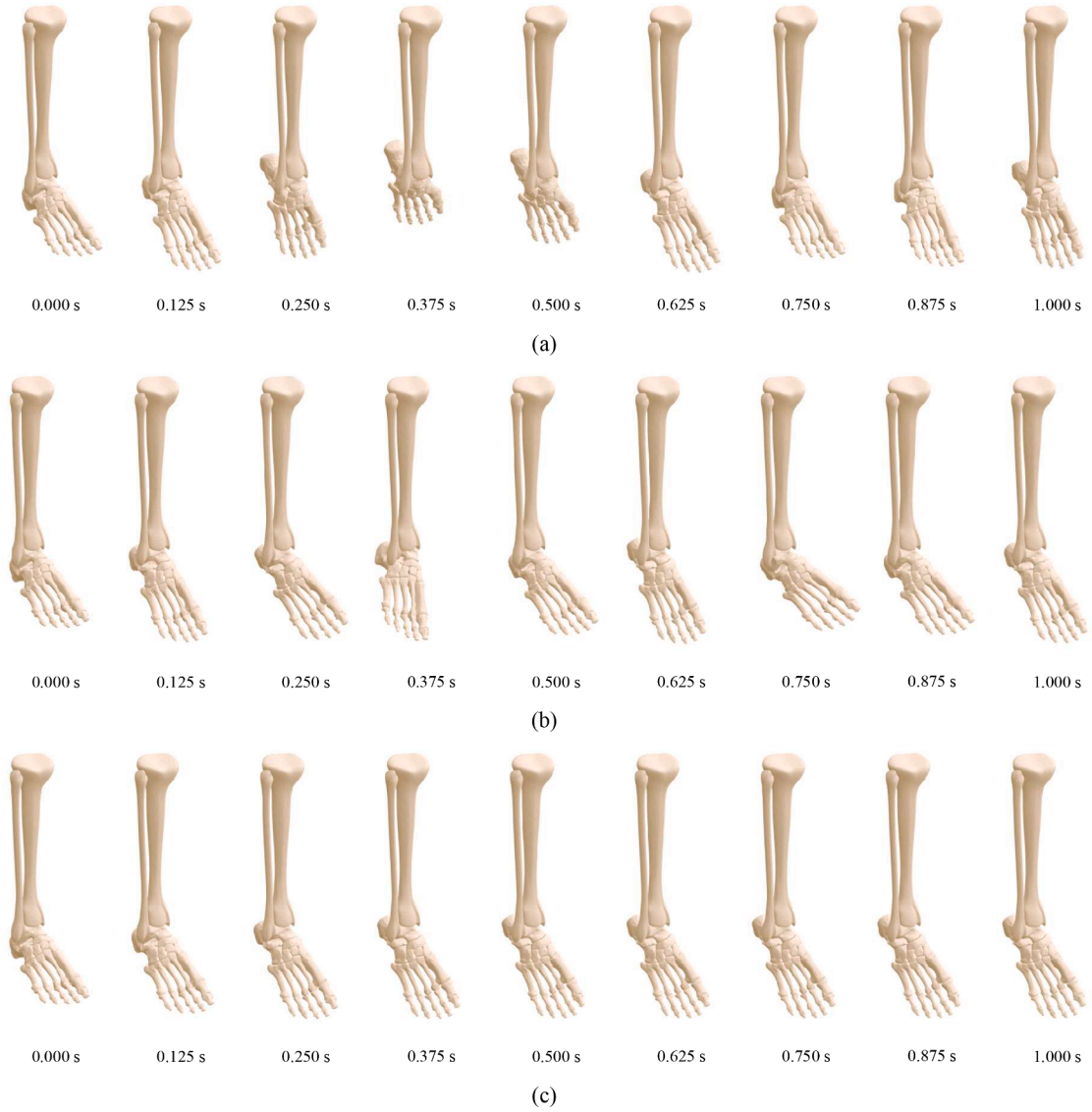

Fig. 13. Snapshot of the movement of the biomechanical model for the first second of simulation (a) subjected to gravitational action only, and with the RoM methodology (b) without and (c) with energy dissipation.

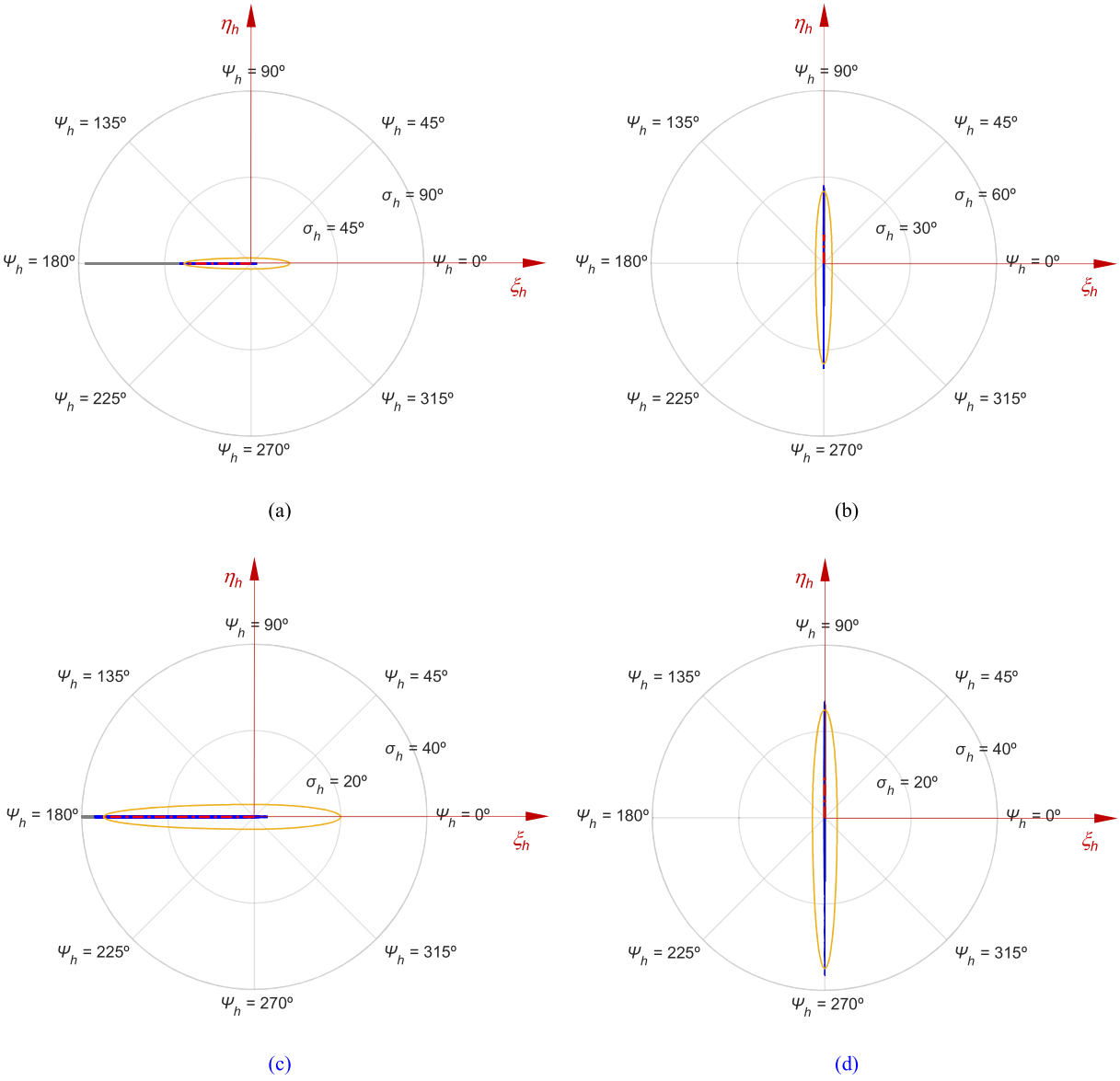

Fig. 14. Variation of the latitude as a function of the longitude for the (a) talocrural and (b) talocalcaneal joints. These figures represent a top view of the joint's local coordinate system: case without RoM (—), RoM without dissipation (---), RoM with dissipation (– · –), and limits of the circumduction cone (—). Figures (c) and (d) depict a zoom of figures (a) and (b), respectively.

dissipative moment provokes significant variations, in relative terms, of the coordinates of the biomechanical model, which reduce the time step required to meet the specified tolerances and proceed with the integration process, significantly decreasing the computational efficiency. In order to ensure that this issue does not affect the analysis, Fig. 16 shows the computational cost for 1 s of simulation only, which represents the simulation time prior to the occurrence of the above-mentioned numerical issues. Observing Fig. 16, the most efficient case is the one in which the RoM methodology is not considered, while the case without energy dissipation is the least efficient one.

6. Concluding remarks

In this work, a methodology to restrict the RoM of joints is applied to the ankle joint complex of the human foot. This methodology can be useful, for instance, in human motion simulation, in planning and optimizing the trajectories of bodies, or in the design of mobility assistive devices or exoskeletons. The ankle joint complex is composed of the talocrural and the talocalcaneal articulations,

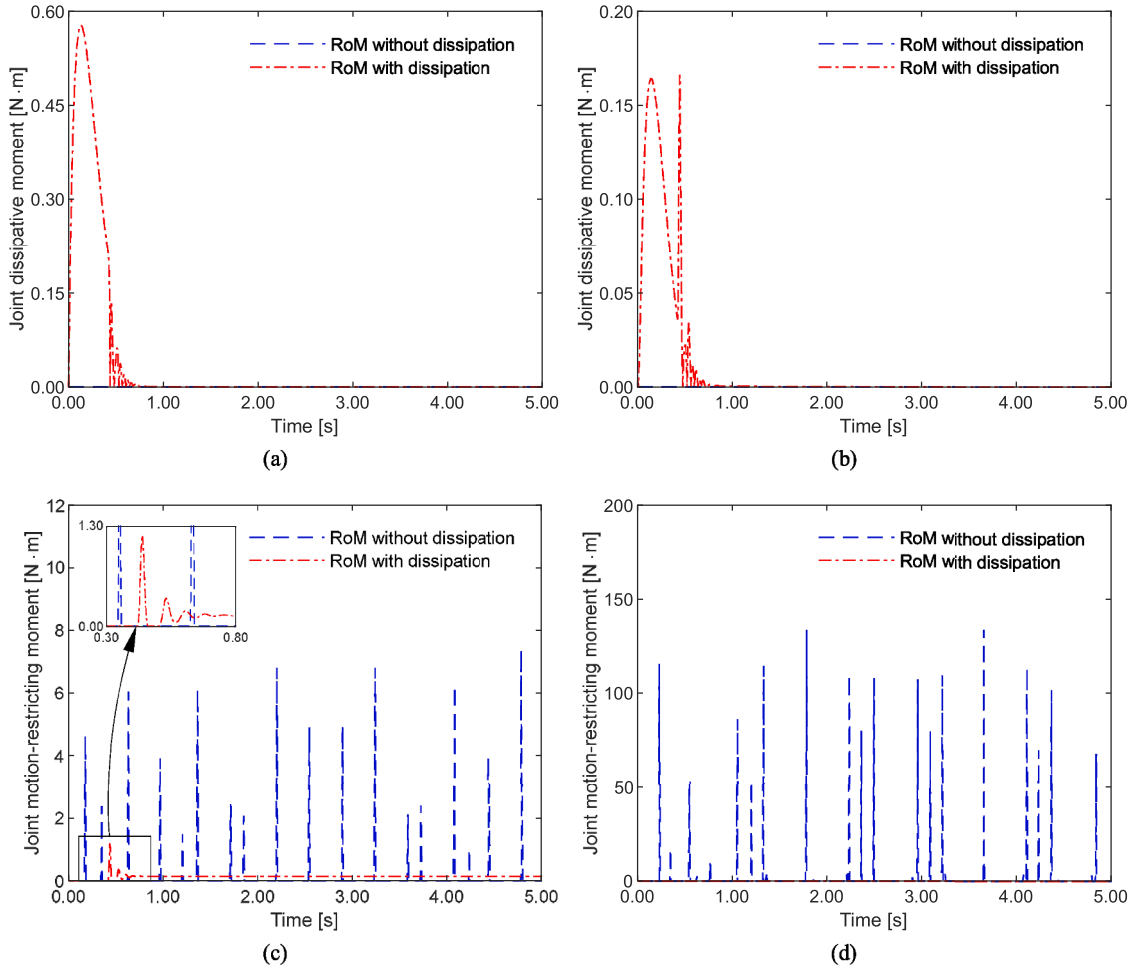

Fig. 15. Evolution of the joint dissipative moment for the (a) talocrural and (b) talocalcaneal joints and of the joint motion-restricting moment for the (c) talocrural and (d) talocalcaneal joints throughout the simulation time.

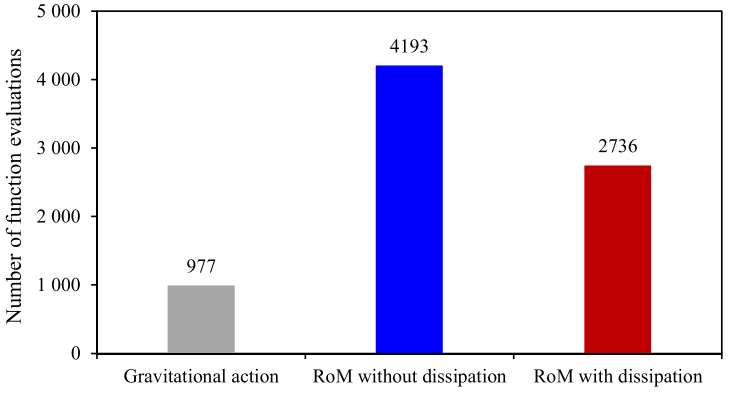

Fig. 16. Computational cost for the biomechanical multibody model for 1 s of simulation.

which allow, respectively, plantarflexion and dorsiflexion, and eversion and inversion of the foot. The RoM methodology applies joint resistance moments to the connected bodies to mimic the resistive and dissipative behavior of the materials constituent of the joint and to prevent unacceptable relative configurations of those bodies. Thus, the joint resistance moments are composed of two terms, namely the joint dissipative moment and the joint motion-restricting moment terms. A three-dimensional biomechanical model of the human leg, main foot and toes is developed under the framework of the multibody systems methodology. The rigid bodies are kinematically connected to each other by means of one revolute joint representing the metatarsophalangeal articulations, and one modified universal joint representing the ankle joint complex. The multibody model has three degrees-of-freedom but, since the metatarsophalangeal joint angle was considered to be locked, in reality the model has two degrees-of-freedom, which include the movements allowed by the ankle joint complex. For the application of the RoM methodology, the modified universal joint can be thought of as two revolute joints, which means that the RoM associated with each joint axis must be restricted independently and two different circumduction cones must be constructed. For both the talocrural and talocalcaneal joints, a detailed description of the application of the RoM methodology is given in this work. The definition of the moving and reference bodies, of the joint's local reference frames and of the circumduction cones for each joint of the ankle joint complex is provided. The estimation of the longitude and latitude, and the calculation of the maximum latitude using the elliptical approach is also described. Due to the fact that, in a modified universal joint, there is a massless link connecting the two bodies, the joint motion-restricting moment is directly applied to the reference body and to the massless link. Thus, a process of force and moment transfer from the massless link to both the moving and reference bodies must be considered and it is explained in detail in this work. From the obtained results, it can be concluded that the methodology correctly restricts the RoM of the ankle joint complex of the human foot and it can be further applied to the dynamic simulation of biomechanical multibody models.

Funding

This work has been supported by Portuguese Foundation for Science and Technology, under the national support to R&D units grant, with the reference project UIDB/04436/2020 and UIDP/04436/2020, as well as through IDMEC, under LAETA, project UIDB/50022/2020. The first author expresses her gratitude to the Portuguese Foundation for Science and Technology through the PhD grant (2021.04840.BD).

CRediT authorship contribution statement

Mariana Rodrigues da Silva: Writing – review & editing, Writing – original draft, Visualization, Validation, Software, Resources, Methodology, Investigation, Formal analysis, Data curation, Conceptualization. **Filipe Marques:** Writing – review & editing, Visualization, Validation, Supervision, Software, Project administration, Methodology, Investigation, Formal analysis, Data curation, Conceptualization. **Miguel Tavares da Silva:** Writing – review & editing, Validation, Supervision, Methodology, Investigation, Data curation, Conceptualization. **Paulo Flores:** Writing – review & editing, Validation, Supervision, Software, Project administration, Methodology, Investigation, Data curation, Conceptualization.

Declaration of competing interest

The authors declare that they have no known competing financial interests or personal relationships that could have appeared to influence the work reported in this paper.

Data availability

Data will be made available on request.

References

[1] M.R. Silva, F. Marques, M.T. Silva, P. Flores, A comprehensive review on biomechanical modeling applied to device-assisted locomotion, Arch. Comput. Method. Eng. 30 (2023) 1897–1960, https://doi.org/10.1007/s11831-022-09856-y.
[2] I. Roupa, M.R. Silva, F. Marques, S.B. Gonçalves, P. Flores, M.T. Silva, On the modeling of biomechanical systems for human movement analysis: a narrative review, Arch. Comput. Method. Eng. 29 (2022) 4915–4958, https://doi.org/10.1007/s11831-022-09757-0.
[3] M. Silva, B. Freitas, R. Andrade, Ó. Carvalho, D. Renjewski, P. Flores, J. Espregueira-Mendes, Current Perspectives on the Biomechanical Modelling of the Human Lower Limb: a Systematic Review, Arch. Comput. Method. Eng. 28 (2021) 601–636, https://doi.org/10.1007/s11831-019-09393-1.
[4] C. Quental, F. Simões, M. Sequeira, J. Ambrósio, J.P. Vilas-Boas, M. Nakashima, A multibody methodological approach to the biomechanics of swimmers including hydrodynamic forces, Multibody Syst. Dyn. 57 (2023) 413–426, https://doi.org/10.1007/s11044-022-09865-6.
[5] M. Febrer-Nafría, R. Pallarès-López, B.J. Fregly, J.M. Font-Llagunes, Prediction of three-dimensional crutch walking patterns using a torque-driven model, Multibody Syst. Dyn. 51 (2021) 1–19, https://doi.org/10.1007/s11044-020-09751-z.
[6] U. Lugrís, J. Carlín, A. Luaces, J. Cuadrado, Gait analysis system for spinal cord-injured subjects assisted by active orthoses and crutches, Proceed. Instit. Mech. Eng. Part K: J. Multi-Body Dyn. 227 (2013) 363–374, https://doi.org/10.1177/1464419313494935.
[7] S.A. Metzler, J.C. Bookwalter, N.P. Eiselstein, SAE Technical Paper, 2007, https://doi.org/10.4271/2007-01-2476.
[8] P.G. Bedewi, K.H. Digges, SAE Technical Paper, 1999, https://doi.org/10.4271/99SC14.
[9] M. Ezati, B. Ghannadi, J. McPhee, A review of simulation methods for human movement dynamics with emphasis on gait, Multibody Syst. Dyn. 47 (2019) 265–292, https://doi.org/10.1007/s11044-019-09685-1.
[10] P. Nikravesh, Computer-aided Analysis of Mechanical Systems, Prentice-Hall, Inc., 1988.

[11] M.R. Silva, F. Marques, M.T. Silva, P. Flores, A comparison of spherical joint models in the dynamic analysis of rigid mechanical systems: ideal, dry, hydrodynamic and bushing approaches, Multibody Syst. Dyn. 56 (2022) 221–266, https://doi.org/10.1007/s11044-022-09843-y.
[12] L. Saraiva, M.R. Silva, F. Marques, M.T. Silva, P. Flores, A review on foot-ground contact modeling strategies for human motion analysis, Mech. Mach. Theory 177 (2022) 105046, https://doi.org/10.1016/j.mechmachtheory.2022.105046.
[13] M.R. Silva, F. Marques, M.T. Silva, P. Flores, A compendium of contact force models inspired by Hunt and Crossley's cornerstone work, Mech. Mach. Theory 167 (2022) 104501, https://doi.org/10.1016/j.mechmachtheory.2021.104501.
[14] A. Ribeiro, J. Rasmussen, P. Flores, L.F. Silva, Modeling of the condyle elements within a biomechanical knee model, Multibody Syst. Dyn. 28 (2012) 181–197, https://doi.org/10.1007/s11044-011-9280-9.
[15] N. Sancisi, X. Gasparutto, V. Parenti-Castelli, R. Dumas, A multi-body optimization framework with a knee kinematic model including articular contacts and ligaments, Meccanica 52 (2017) 695–711, https://doi.org/10.1007/s11012-016-0532-x.
[16] S. Duprey, A. Naaim, F. Moissenet, M. Begon, L. Chèze, Kinematic models of the upper limb joints for multibody kinematics optimisation: an overview, J. Biomech. 62 (2017) 87–94, https://doi.org/10.1016/j.jbiomech.2016.12.005.
[17] C. Quental, J. Folgado, J. Ambrósio, J. Monteiro, A multibody biomechanical model of the upper limb including the shoulder girdle, Multibody Syst. Dyn. 28 (2012) 83–108, https://doi.org/10.1007/s11044-011-9297-0.
[18] M.R. Silva, F. Marques, M.T. Silva, P. Flores, A new skeletal model for the ankle joint complex, Multibody Syst. Dyn. 60 (2024) 27–63, https://doi.org/10.1007/s11044-023-09955-z.
[19] G.T. Yamaguchi, Dynamic Modeling of Musculoskeletal Motion: A Vectorized Approach for Biomechanical Analysis in Three Dimensions, Springer, Boston, 2006.
[20] F. Anderson, M. Pandy, A dynamic optimization solution for vertical jumping in three dimensions, Comput. Method. Biomech. Biomed. Eng. 2 (1999) 201–231, https://doi.org/10.1080/10255849908907988.
[21] A. Szczęsna, Verification of the blobby quaternion model of human joint limits, Biomed. Signal Process. Control 39 (2018) 130–138, https://doi.org/10.1016/j.bspc.2017.07.029.
[22] M. Engell-Nørregård, S. Niebe, K. Erleben, A joint-constraint model for human joints using signed distance-fields, Multibody Syst. Dyn. 28 (2012) 69–81, https://doi.org/10.1007/s11044-011-9296-1.
[23] M.R. Silva, F. Marques, M.T. Silva, P. Flores, An improved methodology to restrict the range of motion of mechanical joints, Nonlinear Dyn. 112 (2024) 4227–4256, https://doi.org/10.1007/s11071-023-09208-w.
[24] J. McKeon, M. Hoch, The ankle-joint complex: a kinesiologic approach to lateral ankle sprains, J. Athl. Train. 54 (2019) 589–602, https://doi.org/10.4085/1062-6050-472-17.
[25] M. Fukano, T. Fukubayashi, S. Banks, Sex differences in three-dimensional talocrural and subtalar joint kinematics during stance phase in healthy young adults, Hum. Mov. Sci. 61 (2018) 117–125, https://doi.org/10.1016/j.humov.2018.06.003.
[26] C. Brockett, G. Chapman, Biomechanics of the ankle, Orthop. Trauma 30 (2016) 232–238, https://doi.org/10.1016/j.mporth.2016.04.015.
[27] S. Standring, Gray's Anatomy: the Anatomical Basis of Clinical Practice, 40th Ed., Elsevier Health Sciences UK, 2008.
[28] B. Pereira, R. Andrade, J. Espregueira-Mendes, R. Marano, X. Oliva, J. Karlsson, Current concepts on subtalar instability, Orthop. J. Sport. Med. 9 (2021) 232596712110213, https://doi.org/10.1177/23259671211021352.
[29] F.C. Anderson, M.G. Pandy, A dynamic optimization solution for vertical jumping in three dimensions, Comput. Method. Biomech. Biomed. Eng. 2 (1999) 201–231, https://doi.org/10.1080/10255849908907988.
[30] D. Neumann, Kinesiology of the Musculoskeletal System: Foundations for Rehabilitation, Second Ed., Mosby - Elsevier, 2013 https://doi.org/10.1016/B978-0-323-03989-5.00015-8.
[31] R. Isman, V. Inman, Anthropometric studies of the human foot and ankle, Bull. Prosthet. Res. (1969).
[32] R.G. Budynas, J.K. Nisbett, Mechanical Engineering - Shigley's Mechanical Engineering Design, Eight Ed., The McGraw−Hill Companies, Inc., 2006.
[33] R.L. Mott, E.M. Vavrek, J. Wang, Machine Elements in Mechanical Design, Sixth Ed., Pearson Education, Inc., 2018.
[34] P. Flores, Concepts and Formulations for Spatial Multibody Dynamics, Springer International Publishing, 2015, https://doi.org/10.1007/978-3-319-16190-7.
[35] F. Marques, I. Roupa, M.T. Silva, P. Flores, H.M. Lankarani, Examination and comparison of different methods to model closed loop kinematic chains using Lagrangian formulation with cut joint, clearance joint constraint and elastic joint approaches, Mech. Mach. Theory 160 (2021) 104294, https://doi.org/10.1016/j.mechmachtheory.2021.104294.
[36] M.R. Silva, F. Marques, M.T. Silva, P. Flores, Modelling Spherical Joints in Multibody Systems, in: M. Pucheta, A. Cardona, S. Preidikman, R. Hecker (Eds.), Multibody Mechatronic Systems. MuSMe 2021. Mechanisms and Machine Science, 110, Springer, Cham, 2022, pp. 85–93, https://doi.org/10.1007/978-3-030-88751-3_9.
[37] M. Khoshnazar, M. Dastranj, A. Azimi, M.M. Aghdam, P. Flores, Application of the Bezier integration technique with enhanced stability in forward dynamics of constrained multibody systems with Baumgarte stabilization method, Eng. Comput. (2023), https://doi.org/10.1007/s00366-023-01884-x.
[38] P. Flores, MUBODYNA - A MATLAB Program For Dynamic Analysis of Spatial Multibody Systems, University of Minho, Guimarães, Portugal, 2012.
[39] M.R. Silva, F. Marques, M.T. Silva, P. Flores, A New model to study the Talocrural-Talocalcaneal articular complex of the human foot, in: IX International Conference on Computational Bioengineering (ICCB 2022), Lisbon, Portugal, 2022.
[40] S. Siegler, J. Toy, D. Seale, D. Pedowitz, New observations on the morphology of the talar dome and its relationship to ankle kinematics, Clin. Biomech. 29 (2014) 1–6, https://doi.org/10.1016/j.clinbiomech.2013.10.009.
[41] M.L. Audu, D.T. Davy, The Influence of Muscle Model Complexity in Musculoskeletal Motion Modeling, J. Biomech. Eng 107 (1985) 147–157, https://doi.org/10.1115/1.3138535.
[42] D.T. Davy, M.L. Audu, A dynamic optimization technique for predicting muscle forces in the swing phase of gait, J. Biomech. 20 (1987) 187–201, https://doi.org/10.1016/0021-9290(87)90310-1.
[43] M.P.T. Silva, J.A.C. Ambrósio, M.S. Pereira, Biomechanical model with joint resistance for impact simulation, Multibody Syst. Dyn. 1 (1997) 65–84, https://doi.org/10.1023/A:1009700405340.
[44] I. Kapandji, The Physiology of Joints. Volume 1: The Upper Extremity, Churchill Livingstone, London, UK, 1974.
[45] J. Panero, M. Zelnik, Human Dimension and Interior Space - A Source Book of Design Reference Standards, Watson-Guptill Publications, 1979.
[46] M.P.T. Silva, J.A.C. Ambrósio, M.S. Pereira, A multibody approach to the vehicle and occupant integrated simulation, Int. J. Crashworthin. 2 (1996) 73–90, https://doi.org/10.1533/cras.1997.0036.
[47] A. Nasr, S. Bell, J. McPhee, Optimal design of active-passive shoulder exoskeletons: a computational modeling of human-robot interaction, Multibody Syst. Dyn. 57 (2023) 73–106, https://doi.org/10.1007/s11044-022-09855-8.
[48] H. Hatze, The complete optimization of a human motion, Math. Biosci. 28 (1976) 99–135, https://doi.org/10.1016/0025-5564(76)90098-5.
[49] E.J. Rouse, L.J. Hargrove, E.J. Perreault, T.A. Kuiken, Estimation of human ankle impedance during the stance phase of walking, IEEE Transact. Neur. Syst. Rehabilit. Eng. 22 (2014) 870–878, https://doi.org/10.1109/TNSRE.2014.2307256.
[50] A.L. Shorter, E.J. Rouse, Mechanical impedance of the ankle during the terminal stance phase of walking, IEEE Transact. Neur. Syst. Rehabilit. Eng. 26 (2018) 135–143, https://doi.org/10.1109/TNSRE.2017.2758325.